Growth of necrotic cores in atherosclerotic plaque

Pak-Wing Fok

Department of Mathematical Sciences, University of Delaware,
DE 19716, USA
pakwing@udel.edu

Plaques are fatty deposits that grow mainly in arteries and develop as a result of a chronic inflammatory response. Plaques are characterized as 'vulnerable' when they have large internal regions of necrosis and are heavily infiltrated by macrophages. The particular composition of a vulnerable plaque renders it susceptible to rupture, which releases thrombogenic agents into the bloodstream and can result in myocardial infarction. In this paper, we propose a mathematical model to predict the development of a plaque's necrotic core. By solving coupled reaction-diffusion equations for macrophages and dead cells, we focus on the joint effects of hypoxic cell death and chemoattraction to oxidized low-density lipoprotein (Ox-LDL), a molecule that is strongly linked to atherosclerosis. We do not model the mechanical properties of the plaque, its growth or rupture. Our model predicts cores that have approximately the right size and shape when compared to ultrasound images. Because our model is linear and autonomous, normal mode analysis and subsequent calculation of the smallest eigenvalue allow us to compute the times taken for the necrotic core to form. We find that the spatial distribution of Ox-LDL within the plaque determines not only the placement and size of cores, but their time of formation. Although plaques are biochemically complex, our study shows that certain aspects of their composition can be predicted and are, in fact, governed by simple physical models.

Keywords: plaque; atherosclerosis; necrosis.

1. Introduction

According to the American Heart Association, cardiovascular disease (CVD) affected about 80 million Americans in 2006 and was responsible for 800,000 deaths. About 35% of all deaths in that year were caused by CVD. The treatment of heart disease is a critically important issue and an outstanding problem in health and medicine.

One common form of CVD is atherosclerosis which is a 'furring' of the artery walls leading to a narrowing of the vessel lumen. It was originally thought that plaque build-up would make patients more susceptible to myocardial infarction (MI) or heart attacks. However, doctors now think that the 'rupture' of certain plaques called thin-capped fibroatheromas (TCFAs) or 'vulnerable plaques' are responsible for most fatalities. In one study (Davies, 1992), 73% of all deaths from MI were caused by plaque rupture. This has led to the definition and characterization of vulnerable plaque (Virmani *et al*., 2007), which is thought to be the major culprit behind MIs. Their study is the focus of this paper.

Vulnerable plaques are characterized by a thin fibrous cap and a necrotic core consisting of lipids, dead cells and calcification. Plaques grow as a result of the body's inflammatory response. Specifically, high concentrations of low-density lipoprotein (LDL) are found in the blood of people who engage in a high-fat diet. LDL is absorbed by endothelial tissue that lines the interior surface of all blood
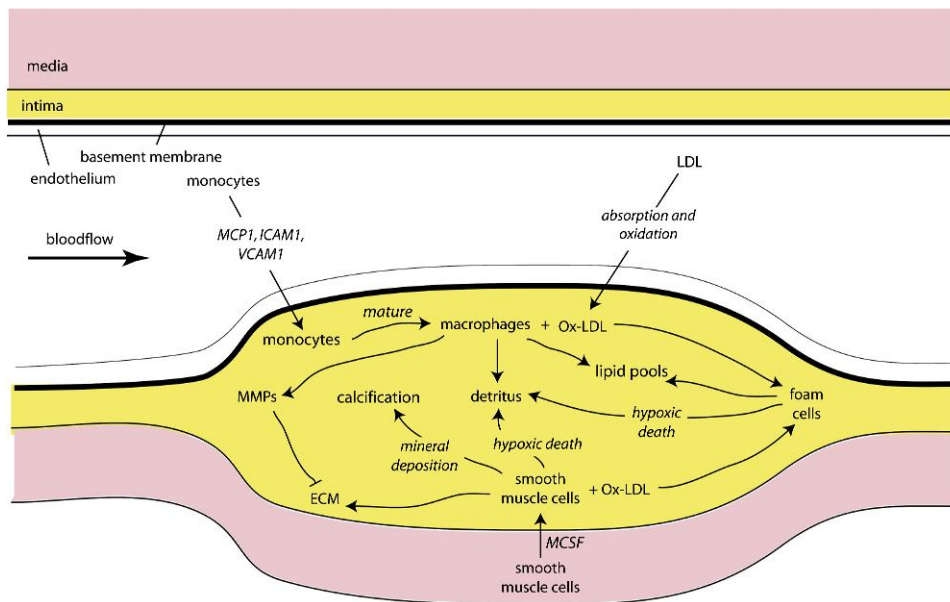
P.W. FOK

FIG. 1. Important biochemical processes in plaque growth. The plaque is shown as a swelling in the intimal region of the artery. MCP1, macrophage chemotactic protein 1.

vessels and diffuses into the intima. There they can then be oxidized by free radicals to form a family of compounds called Ox-LDL. When macrophages phagocytose Ox-LDL, they turn into the foam cell phenotype (Shiffman *et al*., 2000; Fig. 1). Smooth muscle cells (SMCs) can also migrate into the plaque from the underlying media. The death of SMCs, foam cells and macrophages all contribute to a necrotic core, one of the defining characteristics of a vulnerable plaque.

The other defining characteristic is a thin fibrous cap which is typically <65 μm (Virmani *et al*., 2000, 2007; Vengrenyuk *et al*., 2006). The major constituent of the cap is extracellular matrix (ECM). Excretion of certain compounds called matrix metalloproteinases (MMPs) by macrophages and foam cells degrade the ECM in the cap (Shah, 2003), causing it to thin. A vulnerable plaque is more susceptible to rupture due to its thin cap and necrotic core. Upon rupture, tissue factor is released into the bloodstream causing thrombosis and, in many cases, MI. This complicated sequence of events raises some simple — but important — questions. Can we predict how plaques grow? What are the main biological processes that determine the growth rate? Can their growth be suppressed? Can the formation time for vulnerable plaque be predicted?

In this paper, we propose a biochemical model to describe the growth of a vulnerable plaque's necrotic core. We ignore blood flow, mechanical stresses within the plaque and remodelling in the artery walls (treating them as static). Because our focus is on the biochemistry that occurs inside a plaque, we do not consider plaque rupture. The model consists of a system of partial differential equations (PDEs) that accounts for the effects of cell diffusion, death and chemotaxis. Although our equations make some simplifications about the underlying processes that govern plaque growth, they nevertheless predict core shapes and sizes that are consistent with photographs from the medical literature. Our main findings are that (i) Ox-LDL chemotaxis can drive core growth, (ii) the spatial distribution of Ox-LDL within

the plaque determines how rapidly cores develop and (iii) regions of the artery that are oxygen deficient help to 'suppress' core growth.

2. Background

2.1 *Plaque rupture and composition models*

The mechanisms behind plaque rupture are only just beginning to be understood. In plaques, a fibrous 'cap' physically separates the the plaque's contents (lipids, necrotic material, etc.) from the blood-stream. The propensity for a plaque to rupture depends largely on the properties of the cap: vulnerable plaques have thin caps which are more likely to tear than thick ones. Also, vulnerable plaques are highly calcified, resulting in increased cap stiffness and stress. Because necrotic cores cannot sustain large mechanical stresses, which must be born by the cap, the composition of a vulnerable plaque is crucial in determining its overall mechanical integrity.

Although biomechanical models of the artery are important, it is also imperative that models of plaque composition are studied and developed. These should explicitly account for the time evolution of different plaque components and should be able to predict the organization within a plaque. Ibragimov *et al.* (2005) propose a system of PDEs for SMCs, macrophages, debris, LDL, Ox-LDL and chemoattractant. This model was solved in an annulus and was able to capture some aspects of plaque formation such as the isolation of a lesion by SMCs. Ougrinovskaia *et al.* (2010) neglect spatial structure within the plaque and use an ordinary differential equation system to describe lipid and macrophage dynamics. They find that their model either yields stable steady states or unbounded solutions for long times. Calvez *et al.* (2010) propose a very detailed PDE model that couples blood flow to LDL/Ox-LDL concentration and immune cells. One novelty in their model is the introduction of LDL fluxes that depend on the wall shear stress. In comparison with these existing studies, the main strength of our model is that we have found numerical values for most of our parameters and therefore can make concrete predictions for cell numbers, time for plaque formation and so on. Our model is also simple enough that we can generate results in a reasonable amount of time and compare predictions with images from arterial cross sections.

2.2 *Biochemistry and the role of oxidized lipids*

The formation of plaque is a complex process, involving inflammation, leucocyte transport and fluid–structure interactions (see Fig. 1 for a summary of the main biological processes). Plaque thickness is usually on the order of millimetres but plaques can also extend along an artery for centimetres. It is thought that TCFAs take decades to fully form. However, innocuous precursors to a TCFA such as the 'intimal thickening' have actually been found in embryos, and it is unclear whether the transition to a full-fledged TCFA occurs over many decades or whether intimal thickenings lie dormant during that time and metastasize later on. Increase of plaque mass is mainly attributed to a flux of monocytes from the bloodstream and SMCs from the media. Macrophages can transform into foam cells upon consuming oxidized lipoproteins such as Ox-LDL. *In vitro* evidence (Henrikson *et al.*, 1981) suggests that Ox-LDL can be produced by endothelial cells when they are incubated with its native form, LDL. However, when antioxidant levels are low, Ox-LDL can also be produced when LDL reacts with reactive oxygen species. At the same time, SMCs migrate into the intima, attracted by inflammation and associated growth factors such as macrophage colony-stimulating factor (MCSF), elaborate ECM and are mainly responsible for producing calcium deposits within the plaque. In turn, macrophages secrete a suite of MMPs that degrade the ECM. Finally, cells within the plaque can die due to lack of oxygen. After the cells die, their bodies form the necrotic core, one of the defining characteristics of vulnerable plaque.

In 1815, Joseph Hodgson (Acierno, 1994) claimed that atherosclerosis was an inflammatory disease occurring in the intima. However, later experiments by Anitschkow & Chalatow (1913) showed that the arteries of rabbits that were fed a high cholesterol diet contained lipid deposits. As a result, the inflammation theory was temporarily laid to rest until the late 1900s when Ross (1986) unified both theories by explaining the role of oxidized lipids in the context of inflammation. It is now generally agreed (Virmani *et al.*, 2007) that plaque growth is the result of chronic inflammation within blood vessels. Macrophages play a key role in the body's immune response by seeking out and engulfing foreign bodies and pathogens. However, macrophages also play an important role in metabolizing lipids. The highly complex response of monocytes and macrophages in the presence of oxidized lipoproteins such as Ox-LDL is particularly important and an area of active research (Shiffman *et al.*, 2000). For example, Ox-LDL is known to be both cytotoxic and a potent chemoattractant (Tsimikas & Witzum, 2000).

'Ox-LDL' refers to a family of different molecules including free cholesterol, cholesterol esters and phospholipids. These molecules could be in various states of oxidation and have different chemical properties. Minimally modified and native LDL are generally not recognized by macrophage receptors and are not consumed in large amounts. However, 'heavily oxidized' LDL is recognized by scavenger receptors (Tsimikas & Witzum, 2000) and is preferentially endocytosed. Upon consuming large quantities of Ox-LDL, macrophages transform into foam cells, so-called because of their appearance: it is possible to see the foamy lipid droplets inside the cell under a light microscope. Conversion to the foam cell phenotype is probably a continuous process reflecting a gradual accumulation of Ox-LDL. Foam cells appear to be less mobile than normal macrophages. Shiffman *et al.* (2000) showed that certain integrins, responsible for adhesion to ECM, are upregulated in foam cells.

2.3　Blood flow

Although we do not include fluid mechanics in our model, blood flow does affect the rate at which macrophages penetrate the endothelium. Here, we review some of the current literature on the influence of fluid mechanics on atherogenesis.

Many theoretical studies and detailed simulations (Zohdi *et al.*, 2004; Korn & Schwarz, 2008; Ma *et al.*, 2010; Bailey *et al.*, 2007) have focused on how shear stress affects components of the leucocyte adhesion cascade (LAC). At a basic level, the LAC involves four steps. First, monocytes are captured by selectin molecules expressed on the surface of the endothelium. Second, the monocytes roll along the surface detaching from selectins on the trailing edge while adhering to them at the leading one. Third, monocytes become firmly attached onto the endothelium through integrins. Finally, transmigration through the endothelium occurs in the presence of a chemoattractant. The third step of the LAC is mediated by vascular cell adhesion molecule 1 (VCAM1) and intercellular adhesion molecule 1 (ICAM1) (Walpola *et al.*, 1995). Monocytes mature into macrophages once they are in the intima.

Atherosclerotic lesions do not develop uniformly within the coronary tree. Instead, they tend to form at specific locations, e.g. at branch points or in other regions where the flow is far from laminar. Understanding how haemodynamics affects atherogenesis is an area of active study and there are many theories for how blood flow alters general properties of endothelial cells (ECs). For example Chatzizisis *et al.* (2007) argued that pulsatile blood flows with a low time-averaged wall shear stress ($\lesssim 10$–12 dynes/cm^2) — referred to as 'low endothelial shear stress' or low ESS — are responsible for many atherogenic processes including attenuation of nitric oxide production and promotion of LDL uptake. Hsiai *et al.* (2001) focused on the effects of the slew rate (the time rate of change of shear stress) for ECs that were treated with Oxidized 1-palmitoyl-2-arachidonoyl-*sn*-glycero-3-phosphorylcholine

(Ox-PAPC), a component of minimally modified LDL. They considered three different conditions: high slew rate flows, low slew rate flows and oscillatory flows. Both slew flows were set to have the same (positive) time-averaged shear stress, while the oscillatory flow had, by definition, a zero time-averaged shear stress. Compared to no-flow conditions, the authors found that a low slew rate slightly decreased the number of bound monocytes and a high slew rate greatly decreased the number. However, oscillatory flows actually increased the number of bound monocytes: the implication is that oscillatory flows promote inflammation and atherogenesis. Walpola *et al.* (1995) performed *in vivo* experiments to investigate how the adhesion molecules VCAM1 and ICAM1 are regulated in response to different levels of (time averaged) shear stress. By surgically altering carotid arteries in rabbits, they were able to increase the shear stress in some vessels and decrease the shear stress in others (compared to control rabbits). They observed that low shear stress downregulated ICAM1 expression but high shear stress upregulated it. For VCAM1, high shear slightly increased the molecule expression but low shear stress greatly increased it. This survey of some representative studies suggests that although mixed results arise due to differences in experimental procedures, their common, ultimate goal is to understand the coupling between mechanical stress and gene expression in ECs.

3. Model for core growth

Necrotic cores may develop as coherent masses at the centre of the plaque because of hypoxia: cells that are far from the lumen (and hence from the bloodstream) die due to lack of oxygen; a similar process occurs in large tumours (Greenspan, 1972; Byrne, 2010). Cell death[1] and necrosis are different phenomena. Liver cells that are deprived of oxygen undergo cell death after about 150 min (Majno & Joris, 1995) but only become 'necrotic' after 12–24 h: at this stage irreversible changes —such as chromatin breakdown and cytoplasm condensation —have occurred in the cell; these changes are visible under a light microscope long after cell death. As discussed in Section 2, many complex processes occur as plaque develops. To formulate our model, we make a number of simplifications.

First, there are modelling assumptions relating to the geometry of the problem. We assume that the plaque's axial length is much larger than its transverse length (see Fig. 2(a)). We also assume that different cross sections of the plaque are similar to each other in composition and therefore use a 2D model to simplify our analysis. Furthermore, the blood vessel has already undergone 'intimal thickening', a condition corresponding to the 'normal accumulation of SMCs in the intima in the absence of lipid or macrophage foam cells' (Virmani *et al.*, 2000). A blood vessel with intimal thickening appears to be fairly asymmetric with some stenosis causing the lumen to be slightly displaced relative to the basement membrane (Fig. 2(b)). The change from a normal concentric vessel geometry to an eccentric one, typified by intimal thickening, involves an expansion and contraction of the intima and lumen, respectively. This early developmental stage is not treated in our model. Instead, our focus is on the later changes that occur in composition when an already-thickened artery transforms to a TCFA. Any changes in vessel geometry that occur during this process are assumed to be negligible.

Second, there are assumptions that concern the plaque biochemistry: specifically those concerning cell motion and those concerning the dynamics of Ox-LDL. We assume that the flux of monocytes through the endothelial layer is simply proportional to the difference in monocyte concentration across the layer (Fig. 2(c)). Once monocytes are in the intima, they quickly mature into macrophages and climb up gradients in Ox-LDL. If deprived of oxygen, these cells die of hypoxia and nucleate a necrotic core (see Fig. 2(d)). We make no distinction between dead cells and necrotic cells since the time to

---

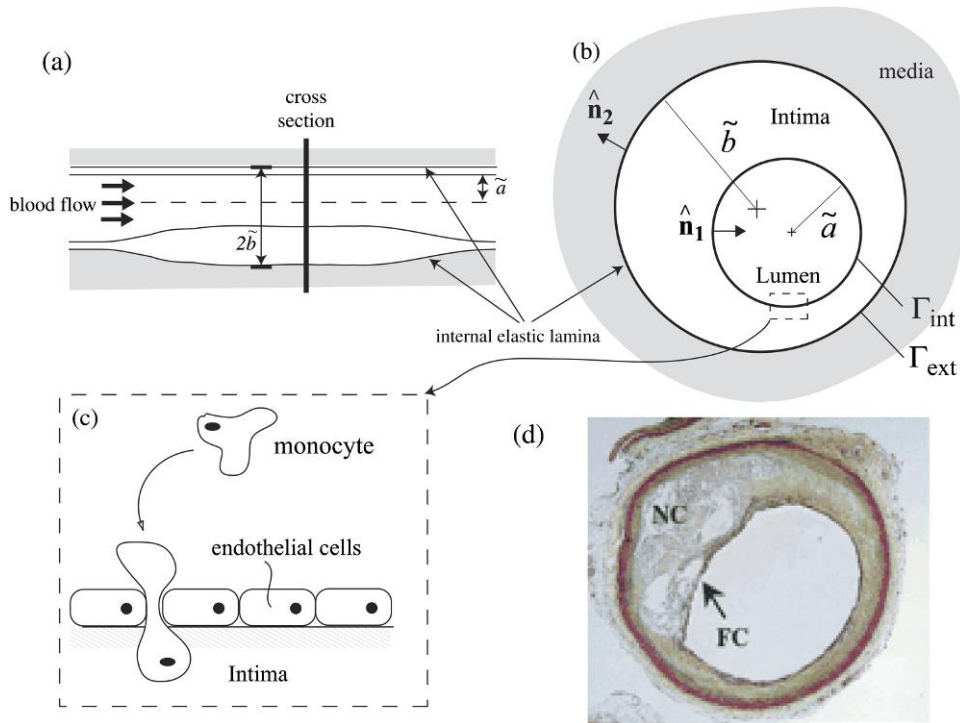[1]Cell death is used here to mean accidental, non-apoptotic cell death.

FIG. 2. (a) An artery with intimal thickening. (b) Cross section of an artery with intimal thickening. $\tilde{a}$ and $\tilde{b}$ are the radii of the lumen and intima. (c) Monocytes penetrate the endothelium, mature into macrophages and die of hypoxia to nucleate the necrotic core. (d) Cross section of a TCFA or 'vulnerable plaque', reproduced with permission from Renu Virmani, Frank D. Kolodgie, Allen P. Burke, Andrew Farb, Stephen M. Schwartz. Lessons From Sudden Coronary Death: A Comprehensive Morphological Classification Scheme for Atherosclerotic Lesions. *Arteriosclerosis, Thrombosis and Vascular Biology*, **20**, 1262–1275. FC, fibrous cap; NC, necrotic core.

cell necrosis is short compared to the time scale of plaque growth. By assuming that all macrophages immediately convert to foam cells upon entering the plaque, we do not need to distinguish between macrophages and foam cells. Our model for Ox-LDL is very simple: we assume it is the dominant chemoattractant in the system and the effect of other chemotactic agents is relatively small. Although Ox-LDL induces a wide range of responses from many cell types, to delineate its effects, we restrict our attention to the case where Ox-LDL acts only as a chemoattractant and does not directly contribute to cell death. In our model, the Ox-LDL distribution within a plaque is time independent. This is mainly because there is very little data on how Ox-LDL levels within a plaque vary over time (potentially, factors such as exercise and diet could affect levels of oxidized lipids within a plaque). In light of our assumptions, the main components in our model are macrophages, dead/necrotic cells, Ox-LDL and oxygen.

In our system, we introduce an Ox-LDL signal deep within the intima and investigate the subsequent inflammatory response and core development. Such a signal could arise (e.g.) when there are elevated levels of free radicals in the vicinity of the plaque. Macrophages are chemotactic to Ox-LDL and respond by moving into the intima. However, they also die due to hypoxic starvation—the further they move into the intima, the less oxygen is available and the more likely they are to undergo ischemic death. This

simple interplay between chemotaxis and cell death is sufficient to produce necrotic cores that have roughly the right size and shape. Our governing equations are

$$\frac{\partial \tilde{Q}}{\partial \tilde{t}} + \tilde{\nabla} \cdot (\tilde{\mu} \tilde{Q} \tilde{\nabla} \tilde{L}) = \tilde{\nu}_1 \tilde{\nabla}^2 \tilde{Q} - \tilde{\gamma}(\tilde{C}) \tilde{Q}, \tag{3.1}$$

$$\frac{\partial \tilde{R}}{\partial \tilde{t}} = \tilde{\nu}_2 \tilde{\nabla}^2 \tilde{R} + \tilde{\gamma}(\tilde{C}) \tilde{Q} - \tilde{\beta}_1 \tilde{R}, \tag{3.2}$$

$$\frac{\partial \tilde{C}}{\partial \tilde{t}} = \tilde{\nu}_3 \tilde{\nabla}^2 \tilde{C} - \tilde{\beta}_2 \tilde{C} - \tilde{\beta}_3 \tilde{C} \tilde{Q}, \tag{3.3}$$

where $\tilde{Q}$, $\tilde{R}$, $\tilde{C}$ are the densities of macrophages, dead cells and concentrations of oxygen inside the plaque, respectively, and $\tilde{\nu}_1$, $\tilde{\nu}_2$ and $\tilde{\nu}_3$ are their diffusivities. While dead cells are not actively mobile, they may still have an effective diffusivity (albeit a small one) due to the motion of neighbouring vital cells. The constant $\tilde{\mu}$ is the macrophage chemotactic coefficient (Keener & Sneyd, 2009b; Keller & Segel, 1971). In our model, we assume that Ox-LDL, represented by $\tilde{L}$ is time independent and its functional form is prescribed later. Time is represented by $\tilde{t}$ and $\tilde{\nabla}$ is the spatial gradient operator.

The function $\tilde{\gamma}(\tilde{C})$ is a macrophage death rate that depends on the local oxygen concentration. Oxygen consumption within the plaque is assumed to come from two sources: $\tilde{\beta}_3$ is the oxygen consumption rate by macrophages, while $\tilde{\beta}_2$ represents the consumption rate by all other cells (e.g. neutrophils and SMCs) whose concentration is assumed to be constant throughout the plaque. It is assumed that these cells are able to freely enter and leave the plaque and access the blood supply. They do not die of hypoxia and do not significantly contribute to necrosis. In contrast, once macrophages enter the plaque, they convert into the foam cell phenotype, become less mobile and are trapped inside. The constant $\tilde{\beta}_1$ represents a constant removal of dead cells from the plaque (e.g. by neutrophils and/or other leucocytes).

For the oxygen-dependent death rate, we follow Owen *et al.* (2004) and use a Hill function of the form

$$\tilde{\gamma}(\tilde{C}) = \tilde{\gamma}_{\min} + (\tilde{\gamma}_{\max} - \tilde{\gamma}_{\min}) \left(\frac{\tilde{C}_{\mathrm{crit}}^m}{\tilde{C}_{\mathrm{crit}}^m + \tilde{C}^m} \right), \tag{3.4}$$

where $\tilde{\gamma}_{\min}$ and $\tilde{\gamma}_{\max}$ are the minimum and maximum death rates, m is a constant Hill coefficient and $\tilde{C}_{\mathrm{crit}}$ is the oxygen concentration such that the death rate is $(\gamma_{\min} + \gamma_{\max})/2$.

Globally high levels of LDL in the bloodstream and the presence of free radicals could result in a localized concentration of Ox-LDL within the intima. We take the Ox-LDL distribution as

$$\tilde{L} = \tilde{L}_0 \exp \left[- \left(\frac{|\tilde{\mathbf{x}} - \tilde{\mathbf{x}}_0|}{\tilde{\delta}} \right)^2 \right], \tag{3.5}$$

where $\tilde{L}_0 = 0.7$ mg/cm^3 is a typical Ox-LDL concentration within the plaque (Van Hoydonck *et al.*, 2003; Nishi *et al.*, 2002). The shape of $\tilde{L}$ is controlled by parameters $\tilde{\delta}$ and $\tilde{\mathbf{x}}_0$, which specify the width of the signal and the position of its maximum, respectively.

The boundary conditions for the macrophages are

$$(\tilde{\mu} \tilde{Q} \tilde{\nabla} \tilde{L} - \tilde{\nu}_1 \tilde{\nabla} \tilde{Q}) \cdot \hat{\mathbf{n}}_1 = \tilde{k}(\tilde{Q} - \tilde{Q}_0), \quad \text{on } \Gamma_{\mathrm{int}}, \tag{3.6}$$

$$(\tilde{\mu} \tilde{Q} \tilde{\nabla} \tilde{L} - \tilde{\nu}_1 \tilde{\nabla} \tilde{Q}) \cdot \hat{\mathbf{n}}_2 = 0, \quad \text{on } \Gamma_{\mathrm{ext}}, \tag{3.7}$$

where $\hat{\mathbf{n}}_1$ and $\hat{\mathbf{n}}_2$ are the outward normals with respect to the domain (Fig. 2(b)). In (3.6), we use a linear kinetic law to relate the flux of macrophages to the difference in concentrations on either side of the endothelium. On the bloodstream side, the concentration is fixed for all time at $\tilde{Q}_0$; a typical value for $\tilde{Q}_0$ is $4 \times 10^5 / \text{cm}^3$ (Keener & Sneyd, 2009b). In (3.7), we assume that the internal elastic lamina acts as an impenetrable barrier.

Similarly, the boundary conditions for oxygen (C) and dead cells (R) at the inner and outer boundaries are

$$\tilde{C} = C_0, \quad \text{on } \Gamma_{\text{int}}, \tag{3.8}$$

$$\hat{\mathbf{n}}_2 \cdot \tilde{\nabla} \tilde{C} = 0, \quad \text{on } \Gamma_{\text{ext}}, \tag{3.9}$$

$$\hat{\mathbf{n}}_1 \cdot \tilde{\nabla} \tilde{R} = 0, \quad \text{on } \Gamma_{\text{int}}, \tag{3.10}$$

$$\hat{\mathbf{n}}_2 \cdot \tilde{\nabla} \tilde{R} = 0, \quad \text{on } \Gamma_{\text{ext}}. \tag{3.11}$$

In (3.8), the oxygen concentration at the endothelium is held fixed at $\tilde{C}_0 = 5.6 \times 10^{-5}$ mol/L (Keener & Sneyd, 2009b). Since the media surrounding the intima in Fig. 2(b) consists of a dense layer of smooth muscle cells, the diffusion coefficient of oxygen in this layer would probably be much smaller than in the intima: equation (3.9) results from imposing flux continuity $\tilde{\nu}_3 \tilde{\nabla} \tilde{C} \cdot \hat{\mathbf{n}}_2 = \tilde{\nu}_{\text{media}} \tilde{\nabla} \tilde{C}_{\text{media}} \cdot \hat{\mathbf{n}}_2$ at the intima–media interface (where $\tilde{\nu}_{\text{media}}$ and $\tilde{C}_{\text{media}}$ are the diffusion coefficient of oxygen and the oxygen concentration in the media) and taking $\tilde{\nu}_{\text{media}}/\tilde{\nu}_3 \to 0$. Equations (3.10) and (3.11) imply that dead cells cannot leave the plaque.

Let $\tilde{a}$ be the radius of the vessel lumen. Using this length scale, the rate constant $\tilde{\beta}_1$ and concentrations $\tilde{Q}_0$, $\tilde{C}_0$ and $\tilde{L}_0$, we introduce dimensionless variables

$$\mathbf{x} = \tilde{\mathbf{x}}/\tilde{a}, \quad t = \tilde{\beta}_1 \tilde{t}, \tag{3.12}$$

$$Q = \tilde{Q}/\tilde{Q}_0, \quad C = \tilde{C}/\tilde{C}_0, \ R = \tilde{R}/\tilde{Q}_0, \quad L = \tilde{L}/\tilde{L}_0, \tag{3.13}$$

resulting in the dimensionless equations

$$\frac{\partial Q}{\partial t} + \mu \nabla \cdot (Q \nabla L) = \nu_1 \nabla^2 Q - \gamma(C) Q, \tag{3.14}$$

$$\frac{\partial R}{\partial t} = \nu_2 \nabla^2 R + \gamma(C) Q - R, \tag{3.15}$$

$$\frac{\partial C}{\partial t} = \nu_3 \nabla^2 C - \beta_2 C - \beta_3 C Q, \tag{3.16}$$

$$\gamma(C) = \gamma_{\min} + (\gamma_{\max} - \gamma_{\min}) \left(\frac{C_{\text{crit}}^m}{C_{\text{crit}}^m + C^m} \right), \tag{3.17}$$

$$L = \exp \left[-\left(\frac{|\mathbf{x} - \mathbf{x}_0|}{\delta} \right)^2 \right], \tag{3.18}$$

where $C_{\text{crit}} = \tilde{C}_{\text{crit}}/\tilde{C}_0$, $\delta = \tilde{\delta}/\tilde{a}$, $\gamma_{\min} = \tilde{\gamma}_{\min}/\tilde{\beta}_1$, $\gamma_{\max} = \tilde{\gamma}_{\max}/\tilde{\beta}_1$, $\mu = \frac{\tilde{\mu}\tilde{L}_0}{\tilde{\beta}_1\tilde{a}^2}$, $\nu_1 = \frac{\tilde{\nu}_1}{\tilde{\beta}_1\tilde{a}^2}$, $\beta_2 = \frac{\tilde{\beta}_2}{\tilde{\beta}_1}$, $\nu_2 = \frac{\tilde{\nu}_2}{\tilde{\beta}_1\tilde{a}^2}$, $\beta_3 = \frac{\tilde{\beta}_3\tilde{Q}_0}{\tilde{\beta}_1}$, $\nu_3 = \frac{\tilde{\nu}_3}{\tilde{\beta}_1\tilde{a}^2}$ and $\mathbf{x}_0 = \tilde{\mathbf{x}}_0/\tilde{a}$. On the inner boundary, the conditions on Γ_{int} are

$$\mathbf{n}_1 \cdot (-\nu_1\nabla Q + \mu Q\nabla L) = k(Q-1), \tag{3.19}$$

$$C = 1, \tag{3.20}$$

$$\mathbf{n}_1 \cdot \nabla R = 0, \tag{3.21}$$

and on the outer boundary, the conditions on Γ_{ext} are

$$\mathbf{n}_2 \cdot (-\nu_1\nabla Q + \mu Q\nabla L) = 0, \tag{3.22}$$

$$\mathbf{n}_2 \cdot \nabla C = 0, \tag{3.23}$$

$$\mathbf{n}_2 \cdot \nabla R = 0, \tag{3.24}$$

where $k = \tilde{k}/(\tilde{\beta}_1\tilde{a})$. The initial conditions for (3.14–3.16) are $Q(\mathbf{x}, 0) \equiv 0$, $R(\mathbf{x}, 0) \equiv 0$ and $C(\mathbf{x}, 0) \equiv 1$. All dimensional and dimensionless parameters in this paper are summarized in Tables 1 and 2.

3.1 Bipolar coordinates

The transformation to Cartesian coordinates (x, y) from bipolar coordinates (τ, σ) is defined by

$$x = \frac{d\sinh\tau}{\cosh\tau - \cos\sigma}, \quad y = \frac{d\sin\sigma}{\cosh\tau - \cos\sigma}, \tag{3.25}$$

TABLE 1 Dimensional constants in (3.1–3.11).

Symbol	Meaning	Units	Value	Reference
$\tilde{\mu}$	MΦ chemotactic coefficient	L^2/T/M/conc.	variable	—
$\tilde{k}$	Monocyte attachment rate	L/T	20 cm/day	Tegoulia & Cooper (2000)
$\tilde{\nu}_1$	Diffusivity of macrophages	L^2/T	9×10^{-3} cm^2/day	Keener & Sneyd (2009b)
$\tilde{\nu}_2$	Diffusivity of dead cells	L^2/T	9×10^{-5} cm^2/day	Owen et al. (2004)
$\tilde{\nu}_3$	Diffusivity of oxygen	L^2/T	9×10^{-1} cm^2/day	Keener & Sneyd (2009a)
$\tilde{\beta}_1$	Dead cell removal rate	1/T	0.1 day^{-1}	Estimated
$\tilde{\beta}_2$	Background O$_2$ consumption	1/T	1.2×10^5 day^{-1}	Keener & Sneyd (2009a)
$\tilde{\beta}_3$	O$_2$ consumption rate by MΦ	1/T/conc.	4×10^{-4} cm^3/day	Hlatky et al. (1988)
$\tilde{a}$	Lumen radius	L	0.2 cm	—
$\tilde{b}$	Intima radius	L	variable	—
$\tilde{\gamma}_{\min}$	Normal MΦ death rate	1/T	0.03 day^{-1}	Estimated
$\tilde{\gamma}_{\max}$	Hypoxic MΦ death rate	1/T	12 day^{-1}	Estimated
$\tilde{L}_0$	Ox-LDL level in plaque	M $\times$ conc.	0.7 mg/cm^3	Nishi et al. (2002)
$\tilde{C}_0$	O$_2$ concentration in blood	conc.	5.6×10^{-5} mol/L	Keener & Sneyd (2009b)
$\tilde{Q}_0$	Monocyte conc. in blood	conc.	4×10^5/cm^3	Alberts et al. (2008)
$\tilde{C}_{\text{crit}}$	Hypoxic O$_2$ concentration	conc.	$0.2 \times \tilde{C}_0$	Owen et al. (2004)

MΦ, macrophage; L, length; T, time; M, mass; conc., concentration. Values were either estimated or taken from the literature: see Appendix 5.

TABLE 2 *Approximate value of dimensionless constants in* (3.14–3.17) *and* (3.30).

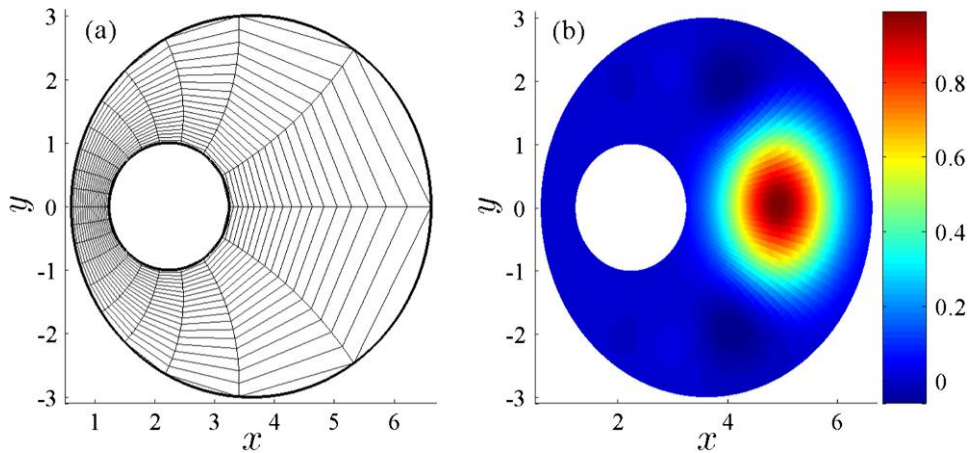| Symbol	Definition	Value
μ	$\tilde{\mu}\tilde{L}_0/(\tilde{\beta}_1\tilde{a}^2)$	Variable
k	$\tilde{k}/(\tilde{\beta}_1\tilde{a})$	1000
ν_1	$\tilde{\nu}_1/(\tilde{\beta}_1\tilde{a}^2)$	2
ν_2	$\tilde{\nu}_2/(\tilde{\beta}_1\tilde{a}^2)$	0.02
ν_3	$\tilde{\nu}_3/(\tilde{\beta}_1\tilde{a}^2)$	200
β_2	$\tilde{\beta}_2/\tilde{\beta}_1$	1.2×10^6
β_3	$\tilde{Q}_0\tilde{\beta}_3/\tilde{\beta}_1$	1600
$\gamma_{\min}$	$\tilde{\gamma}_{\min}/\tilde{\beta}_1$	0.3
$\gamma_{\max}$	$\tilde{\gamma}_{\max}/\tilde{\beta}_1$	120
C_{crit}	$\tilde{C}_{\text{crit}}/\tilde{C}_0$	0.2
r	$\sqrt{\beta_2/\nu_3}$	80

FIG. 3. (a) A 20×20 bipolar grid; (x, y) are dimensionless, defined by (3.25). The $\tau =$ constant level curves of a bipolar coordinate system are non-intersecting eccentric circles of the form $(x - d\coth\tau)^2 + y^2 = d^2/\sinh^2\tau_{\text{int}}$, approximated here with line segments. (b) The (dimensionless) Ox-LDL signal $L(x, y)$ follows (3.18). Here, $\delta = 1$, $\chi = 0.5$ and $d = 2$.

where d controls the eccentricity of the constant-τ level curves (Fig. 3(a))

$$(x - d\coth\tau)^2 + y^2 = \frac{d^2}{\sinh^2\tau}. \tag{3.26}$$

The mesh width becomes larger as τ approaches τ_{ext} and when the angle σ approaches 0. Our domain of solution is $-\pi \leqslant \sigma < \pi$ and $\tau_{\text{ext}} \leqslant \tau \leqslant \tau_{\text{int}}$. The dimensionless inner radius is scaled to 1 so that $\sinh\tau_{\text{int}} = d$. The outer radius $b = \tilde{b}/\tilde{a}$ satisfies $b = d/\sinh\tau_{\text{ext}}$. The centres of the two circular boundaries are located at $(0, d\coth\tau_{\text{int}})$ and $(0, d\coth\tau_{\text{ext}})$.

We introduce the Ox-LDL signal in the thickened part of the intima (Fig. 3(b)). Specifically, the position of the maximum in L is set at $(x_0, 0)$, where x_0 lies between the inner and outer boundaries, i.e.

$$x_0 = P_1 + \chi (P_2 - P_1), \quad 0 \leqslant \chi \leqslant 1, \tag{3.27}$$

$$P_1 = d \coth \tau_{\text{int}} + 1 = \sqrt{1 + d^2} + 1, \tag{3.28}$$

$$P_2 = d (\coth \tau_{\text{ext}} + \operatorname{cosech} \tau_{\text{ext}}) = \sqrt{b^2 + d^2} + b. \tag{3.29}$$

3.2 *Approximation for oxygen concentration*

Since $\beta_3 \ll \beta_2$ in Table 2, the presence of macrophages does not significantly affect the oxygen distribution within the plaque. Also, since β_2 is so large, the oxygen concentration finds its steady-state distribution extremely quickly. Therefore, we can approximate (3.16) with

$$\nabla^2 C - r^2 C = 0, \tag{3.30}$$

where $r = \sqrt{\beta_2 / \nu_3} \gg 1$. Analytic solutions can now be found using singular perturbation. Specifically, we seek solutions to

$$C = \frac{(\cosh \tau - \cos \sigma)^2}{r^2 d^2} \left(\frac{\partial^2 C}{\partial \sigma^2} + \frac{\partial^2 C}{\partial \tau^2} \right), \tag{3.31}$$

$$C = 1, \quad \text{on } \tau = \tau_{\text{int}}, \tag{3.32}$$

$$\frac{\partial C}{\partial \tau} = 0, \quad \text{on } \tau = \tau_{\text{ext}}, \tag{3.33}$$

and obtain

$$C(\tau, \sigma) \sim \exp \left(-\frac{rd(\tau_{\text{int}} - \tau)}{\cosh \tau_{\text{int}} - \cos \sigma} \right), \quad r \gg 1. \tag{3.34}$$

In Table 2, we estimate $r = 80$ with the result that the oxygen concentration rapidly decays away from the vessel lumen. Our final set of equations is

$$\frac{\partial Q}{\partial t} + \mu \nabla \cdot (Q \nabla L) = \nu_1 \nabla^2 Q - \gamma (C) Q, \tag{3.35}$$

$$\frac{\partial R}{\partial t} = \nu_2 \nabla^2 R + \gamma (C) Q - R, \tag{3.36}$$

$$C = \exp \left(-\frac{rd(\tau_{\text{int}} - \tau)}{\cosh \tau_{\text{int}} - \cos \sigma} \right), \tag{3.37}$$

$$L = \exp \left[-\frac{(x - x_0)^2 + y^2}{\delta^2} \right], \tag{3.38}$$

with $\gamma(C)$ defined in (3.17) and x_0 defined in (3.27). The boundary conditions are

$$-v_1 \frac{\partial Q}{\partial \tau} + \mu Q \frac{\partial L}{\partial \tau} = k(Q-1), \quad \text{on } \tau = \tau_{\text{int}}, \tag{3.39}$$

$$-v_1 \frac{\partial Q}{\partial \tau} + \mu Q \frac{\partial L}{\partial \tau} = 0, \quad \text{on } \tau = \tau_{\text{ext}}, \tag{3.40}$$

$$\frac{\partial R}{\partial \tau} = 0, \quad \text{on } \tau = \tau_{\text{int}}, \tau_{\text{ext}} \tag{3.41}$$

and the initial conditions are

$$Q(\tau, \sigma, t = 0) = 0, \tag{3.42}$$

$$R(\tau, \sigma, t = 0) = 0. \tag{3.43}$$

4. Results and Discussion

We solved (3.35–3.41) numerically using finite differences; details of our method can be found in Appendix 5. In our equations, the characteristic crescent-shaped cores often observed in vulnerable plaques arise quite commonly (see Fig. 4 for a qualitative comparison).

Figure 5 shows three snapshots in time of a developing plaque. We see that the macrophage distribution quickly finds its steady state compared to the dead cells. In (a), (c) and (e), the region in the vicinity of the lumen is inflamed with a greater concentration of cells on the thickened side of the
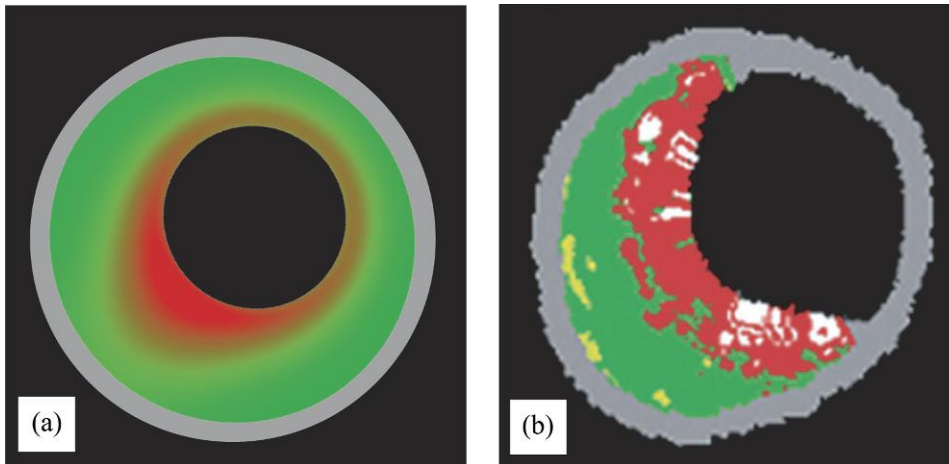

FIG. 4. (a) Typical distribution of necrotic cells generated by our model. Red (Green) represents a larger (smaller) concentration of dead cells. (b) Cross section of artery obtained by intravascular ultrasound (IVUS), reproduced with permission from Sameer K. Mehta, Justin R. McCrary, Andrew D. Frutkin, William J.S. Dolla, Steven P. Marso. (2007). Intravascular ultrasound radiofrequency analysis of coronary atherosclerosis: an emerging technology for the assessment of vulnerable plaque. *European Heart Journal*, **28**, 1283–1288, by permission of the European Society of Cardiology. Colors represent necrotic cells (red), fibrous material (green), fibro-fatty material (yellow) and calcium deposits (white).
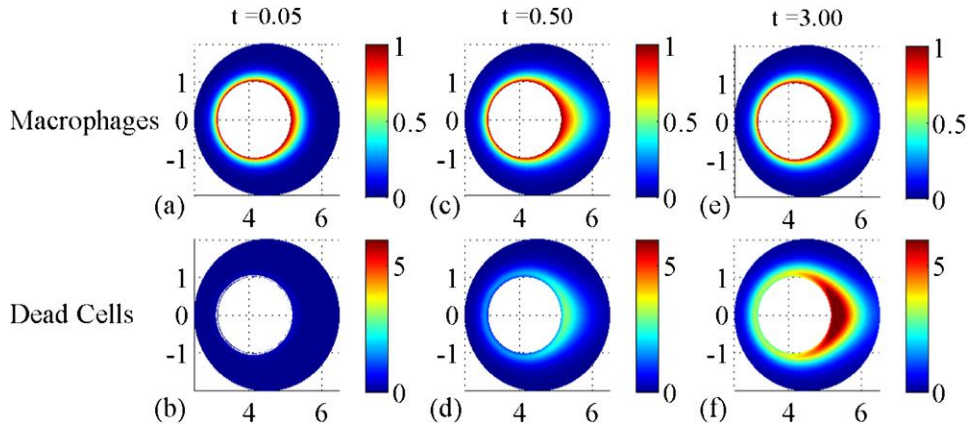
FIG. 5. Growth of necrotic region over time: parameters used were $\mu = 20$, $\nu_1 = 1$, $\nu_2 = 0.01$, $k = 10^3$, $r = 50$, $m = 4$, $\gamma_{\min} = 0.3$, $\gamma_{\max} = 10$, $C_{\text{crit}} = 0.1$, $\delta = 3$, $b = 2$, $d = 4$ and $\chi = 0.7$.

intima. This is due to chemoattraction to Ox-LDL. In this simulation, the Ox-LDL concentration peaks at $(x_0, y_0) \approx (6.1, 0)$. Over time, macrophages climb up the gradient in Ox-LDL and attempt to localize at this point. However, a scarcity of oxygen deep within the intima ensures that the macrophages are actually confined near the lumen. In (f), we see the fully developed crescent-shaped core, characteristic of many vulnerable plaques; its precursor is clearly seen in (d). The positions of the cores in (d) and (f) follow regions of high inflammation in (c) and (e), where the macrophages are highly concentrated. The growth of the core results from a persistent macrophage presence coupled with a high death rate: both γ and Q must be large in (3.36) for R to grow. The crescent core shape arises because the death rate is modulated by the oxygen concentration, which in turn decays radially outward with respect to the lumen. In this simulation, for times $t > 3$, there is no significant change in either the macrophage or dead cell populations and the distributions have reached their steady state to within numerical accuracy.

In Fig. 6, we plot the maximum concentration of dead cells at steady state as a function of relative Ox-LDL location χ and chemotactic parameter μ. Recall from (3.27) that $0 \leqslant \chi \leqslant 1$ is a dimensionless parameter that controls the position of the maximum in L: $\chi = 0$ corresponds to the inner boundary and $\chi = 1$ to the outer one. We find that, for sufficiently large domains ((b) and (c)), there is an intermediate value of χ that gives the most concentrated necrotic cores. The reason is that for small χ, macrophages localize near the lumen where the oxygen concentration is high. Therefore, the death rate is small and necrotic cores are also small and less concentrated. If χ is large, high concentrations of Ox-LDL are too far away and will fail to attract many macrophages. Again, the macrophages will localize near the lumen and the cores will contain few dead cells. For intermediate values of χ, Ox-LDL is sufficiently far away to draw macrophages away from the lumen, but close enough that macrophages still 'see' a sufficiently large gradient. Our results suggest that although the presence of Ox-LDL can nucleate necrotic cores, its location within the intima is important in determining their size, shape and concentration.

Figure 7 shows the steady state of macrophages and dead cells when the chemotactic parameter μ is changed. In Fig. 7(a), the macrophages remain symmetrically confined around the lumen when $\mu = 0$. As μ is increased, they penetrate further into the intima and there is a concomitant production of dead cells (Fig. 7(d) and (f)). We found that decreasing $\gamma_{\max}$ has the same qualitative effect as increasing μ:
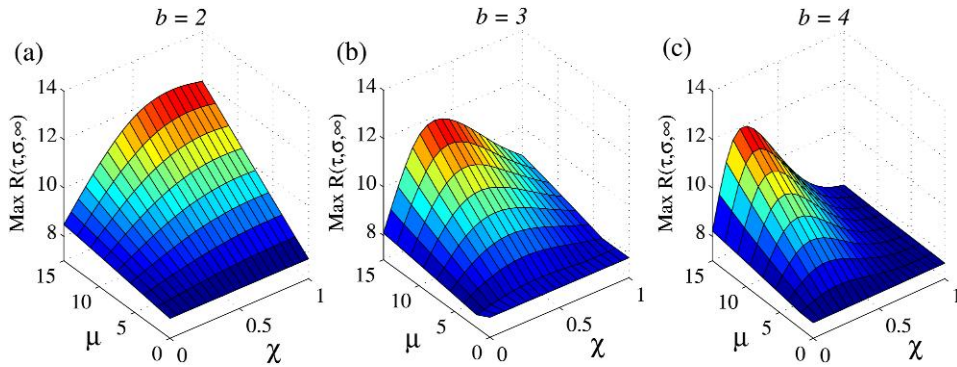
FIG. 6. Maximum dead cell density, (at steady state) as a function of Ox-LDL location χ and chemotactic parameter μ. The parameter b controls the size of the intimal region. (a) $b = 2$, (b) $b = 3$, (c) $b = 4$. Common parameters were $\nu_1 = 1$, $\nu_2 = 0.02$, $k = 10^3$, $r = 50$, $m = 4$, $\gamma_{\min} = 0.3$, $\gamma_{\max} = 20$, $C_{\text{crit}} = 0.1$, $\delta = 2$ and $d = 4$.
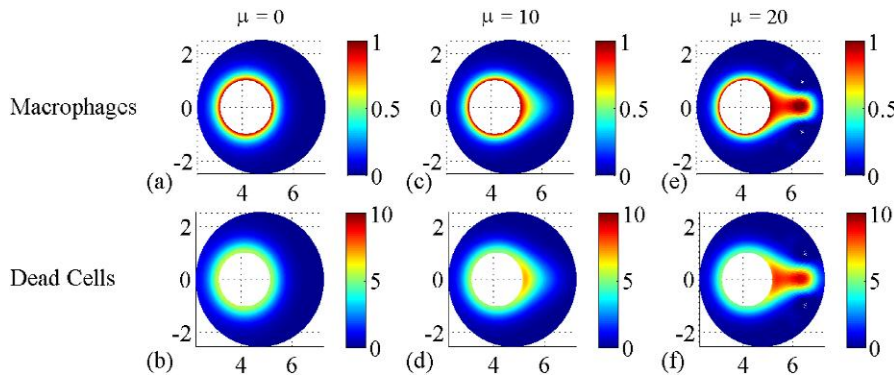

FIG. 7. Core size and shape as a function of macrophage chemotaxis μ. (a, b) $\mu = 0$, (c, d) $\mu = 10$, (e, f) $\mu = 20$. Macrophage densities are represented in the top row, while dead cell densities are shown in the bottom. Common parameters were $\nu_1 = 1$, $\nu_2 = 0.02$, $k = 10^3$, $r = 50$, $m = 4$, $\gamma_{\min} = 0.3$, $\gamma_{\max} = 10$, $C_{\text{crit}} = 0.1$, $\delta = 2$, $b = 2.5$, $d = 4$ and $\chi = 0.7$. Final time of integration was $T = 5$.

larger $\gamma_{\max}$ produces larger necrotic cores with a higher dead cell density. Generally for small values of μ (or large $\gamma_{\max}$), our simulations predict that necrosis will be present only in very thin regions surrounding the lumen. However, in many photographs of arterial cross sections, we see large necrotic cores that effectively fill the entire intima. This observation suggests that the chemotactic parameter $\mu \gg \gamma_{\max}$ which could be realized in (at least) two ways. One possibility is that the death rate is large far away from the lumen, but macrophages are so strongly attracted to Ox-LDL that they nevertheless fill the entire intima. Another possibility is that they can be moderately attracted to Ox-LDL but $\gamma_{\max}$ is artificially lowered within the intima so that $O(1) = \mu \gg \gamma_{\max}$. This second mechanism is discussed in further detail near the end of this section.

　　Figure 8 shows the effect of increasing the macrophage diffusivity ν_1 on the final steady-state distributions. When $\nu = 0.1$, inflammation and necrosis are both localized to a thin region in the thickened
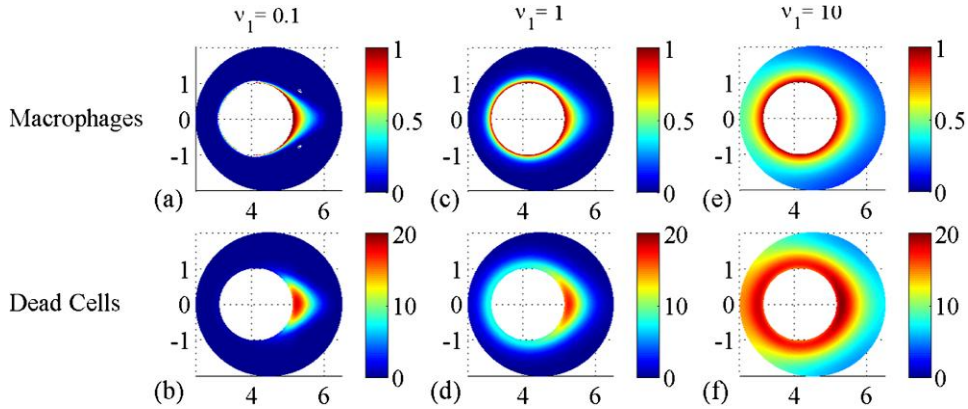
FIG. 8. Core size and shape as a function of macrophage diffusion ν_1. (a,b) $\nu_1 = 0.1$, (c,d) $\nu_1 = 1$, (e,f) $\nu_1 = 10$. Macrophage densities are represented in the top row while dead cell densities are shown in the bottom. Common parameters were $\mu = 20$, $\nu_2 = 0.02$, $k = 10^3$, $r = 50$, $m = 4$, $\gamma_{\min} = 0.3$, $\gamma_{\max} = 30$, $C_{\text{crit}} = 0.1$, $\delta = 2$, $b = 2$, $d = 4$ and $\chi = 0.7$. Final time of integration was $T = 5$.

part of the intima. However, as ν_1 is increased, macrophages become more mobile and one observes a region of inflammation that surrounds the entire lumen. A concentrated crescent-shaped necrotic core can also be seen in the thickened part of the intima. When $\nu_1 = 10$, although macrophages effectively fill the entire domain, they are more concentrated near the oxygen supply. The crescent-shaped necrotic core in (d) has now been replaced with a 'ring' of necrosis. Throughout the rest of the plaque, one sees moderate concentrations of dead cells and detritus.

We now discuss the timescales required for our equations to reach steady state. Because (3.35–3.41) are linear and autonomous, their evolution to steady state is completely determined by their eigenvalues and eigenfunctions. Consider the eigenvalue problem associated with (3.35),

$$S[Q_n] = \lambda_n Q_n, \tag{4.1}$$

$$-\nu_1 \mathbf{n}_1 \cdot \nabla Q_n + (\mu \mathbf{n}_1 \cdot \nabla L - k) Q_n = 0, \quad \text{on } \tau = \tau_{\text{int}}, \tag{4.2}$$

$$-\nu_1 \mathbf{n}_2 \cdot \nabla Q_n + \mu (\mathbf{n}_2 \cdot \nabla L) Q_n = 0, \quad \text{on } \tau = \tau_{\text{ext}}, \tag{4.3}$$

where the operator

$$S[Q] \equiv -\nu_1 \nabla^2 Q + \mu \nabla \cdot (Q \nabla L) + \gamma(\tau, \sigma) Q, \tag{4.4}$$

$\lambda_0 \leqslant \lambda_1 \leqslant \ldots \leqslant \lambda_n \leqslant \ldots$ are the eigenvalues and Q_n are the associated eigenfunctions. We have replaced the inhomogeneous boundary condition (3.39) with (4.2) since eigenvalue problems are defined with homogeneous conditions. A simple substitution in (3.35) converts the homogeneous PDE with inhomogeneous boundary conditions to an inhomogeneous PDE with homogeneous boundary conditions. In (4.4), we use the shorthand $\gamma(\tau, \sigma) \equiv \gamma(C(\tau, \sigma))$. The first four even eigenfunctions (eigenfunctions that are symmetric with respect to σ) are shown in Fig. 9. We only consider even eigenfunctions because the solution to (3.35–3.43) is always even. The eigenfunction corresponding to λ_0 is almost constant everywhere but has a single maximum that coincides with the peak in L. The eigenfunctions for $n > 0$, as expected, show more spatial structure but all feature a maximum or minimum near (x_0, y_0). All eigenfunctions $Q_n(\tau, \sigma)$ were normalized so that $\iint Q_n^2 dA = 1$.
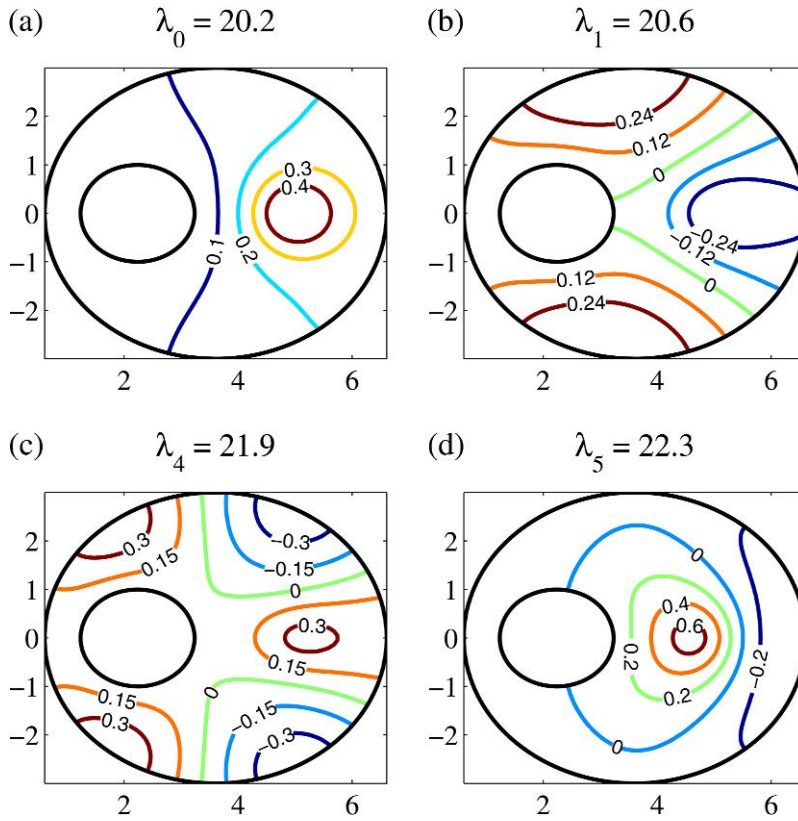
FIG. 9. First four even eigenfunctions of (4.1–4.3) with corresponding eigenvalues (eigenfunctions corresponding to λ_2 and λ_3 are odd). Parameters were $\mu = 1$, $\nu_1 = 1$, $k = 10^3$, $r = 50$, $m = 2$, $\gamma_{min} = 0.01$, $\gamma_{max} = 20$, $C_{crit} = 0.1$, $\delta = 1$, $b = 3$, $d = 2$ and $\chi = 0.5$. A 30×300 grid was used in the calculation. Details of the numerical method can be found in Appendix B.2.

If all the eigenvalues λ_n are positive, then (3.35) and (3.36) have steady states. Any negative eigenvalues $\lambda_n < 0$ correspond to solutions that are unbounded in time, growing like $\exp(-\lambda_n t)$. This instability must be caused by chemotaxis because when $\mu = 0$, the system always has a stable steady state (Appendix B.2). Our model equations can be viewed as a linear approximation of a more complicated, nonlinear model for plaque evolution. When solutions grow exponentially, we expect nonlinear terms of the full model to eventually become important. For example since macrophages have a finite volume, the cell density cannot become arbitrarily large. Finite size effects would come into effect at large t to prevent an explosion in cell density (see Painter & Hillen, 2002 for further details).

When $\lambda_n > 0$ for all n, the solution is a superposition of exponentially decaying modes. The smallest eigenvalue, λ_0, corresponds to the slowest decaying mode and $1/\lambda_0$ gives the time scale for this decay, while at the same time providing a convenient estimate for the time taken for (3.35) to reach steady state. (This estimate was also confirmed by solving the full model (3.35–3.38) for a wide range of parameter values.) In summary, the smallest eigenvalue λ_0 can be used to estimate T_c, the time for the macrophage density to reach steady state:

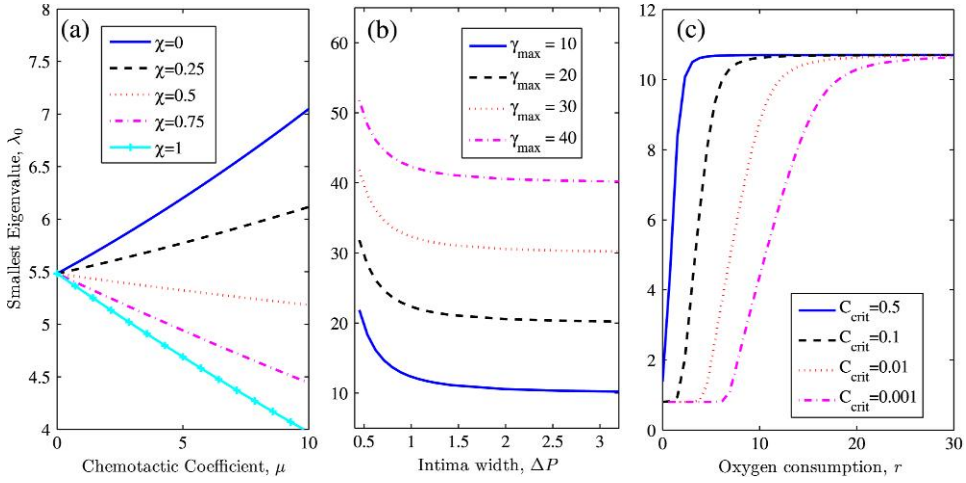$$T_c = \frac{1}{\lambda_0}. \tag{4.5}$$

FIG. 10. Dependence of smallest eigenvalue λ_0 in (4.1–4.3) on chemotaxis, domain size and oxygen consumption rate. (a) λ_0 as a function of the macrophage chemotactic parameter μ for Ox-LDL distributions centred at $(x_0, y_0) = P_1 + \chi(P_2 - P_1)$ (see equation (3.27)). Parameters were $\nu_1 = 5$, $k = 10^3$, $r = 50$, $m = 4$, $\gamma_{\min} = 0.01$, $\gamma_{\max} = 1$, $C_{\mathrm{crit}} = 0.1$, $\delta = 2$ $b = 2$ and $d = 2$. (b) λ_0 as a function of the intima width $\Delta P \equiv P_2 - P_1$ (controlled by the intima radius b) for different hypoxic death rates $\gamma_{\max}$. Parameters were $\mu = 0$, $\nu_1 = 1$, $k = 10^3$, $r = 50$, $m = 4$, $\gamma_{\min} = 0.1$, $C_{\mathrm{crit}} = 0.1$, $\delta = 1$, $d = 2$ and $\chi = 0.5$. (c) λ_0 as a function of oxygen consumption rate r for critical oxygen levels C_{crit}. Parameters were $\mu = 0$, $\nu_1 = 1$, $k = 10^3$, $m = 4$, $\gamma_{\min} = 0.1$, $\gamma_{\max} = 10$, $\delta = 1$, $b = 2$, $d = 1$, $\chi = 0.5$. A $M \times N = 30 \times 300$ grid was used in all computations.

In Fig. 10, we explore the dependence of λ_0 on system parameters. In Fig. 10(a), we plot λ_0 as a function of chemotactic coefficient μ for different values of $0 \leqslant \chi \leqslant 1$, which controls the location of the maximum in L. The dependence is linear for a large range of μ. When Ox-LDL is concentrated near the lumen ($\chi \sim 0$), the system reaches steady state more quickly as μ increases. However, when Ox-LDL is more concentrated deep within the intima ($\chi \sim 1$), steady state is reached more slowly. Our results suggest that the spatial distribution of Ox-LDL within the plaque is important in determining T_c and hence how quickly necrotic cores form.

The dependence of $\lambda_0(\mu)$ on χ can be understood by examining the eigenvalue problem in a 1D model of plaque growth

$$-\nu_1 Q'' + \mu(QL')' + \gamma_{\max} Q = \lambda Q, \quad \text{for } \tau_{\mathrm{int}} < \tau < \tau_{\mathrm{ext}}, \tag{4.6}$$

$$Q = 0, \quad \text{on } \tau = \tau_{\mathrm{int}}, \tag{4.7}$$

$$-\nu_1 Q' + \mu QL' = 0, \quad \text{on } \tau = \tau_{\mathrm{ext}}. \tag{4.8}$$

In this model, we fix the death rate to be $\gamma_{\max}$, a reasonable approximation given that $\gamma \approx \gamma_{\max}$ throughout most of the intima. We also take a homogeneous dirichlet condition for Q since the full condition (3.39) reduces to $Q(\tau_{\mathrm{int}}) = 1$, when $k \gg 1$. In all other aspects, the two models are identical. The main difference is that for the 1D model, we can calculate eigenvalues analytically and the results guide our numerical results and physical understanding in the 2D model.

An asymptotic analysis of the 1D model for $\mu \ll 1$ yields

$$\lambda_0(\mu) = \lambda_0(0) + \mu \lambda_0'(0) + O(\mu^2), \tag{4.9}$$

where

$$\lambda_0(0) = \gamma_{\max} + \nu_1 \left(\frac{\pi}{2\Delta\tau} \right)^2, \tag{4.10}$$

$$\lambda_0'(0) = \frac{2}{\Delta\tau} L'(\tau_{\text{ext}}) \tag{4.11}$$

$$+ \frac{\pi}{\delta^2} \int_0^1 (X - X_0) \exp\left[-\frac{\Delta\tau^2}{\delta^2}(X - X_0)^2 \right] \sin(\pi X)\, dX.$$

In (4.10) and (4.11), the intima width is $\Delta\tau = \tau_{\text{ext}} - \tau_{\text{int}}$ and $X_0 = (x_0 - \tau_{\text{int}})/\Delta\tau$ plays the role of χ. More details of this calculation can be found in Appendix B.2. We can now understand why the position of the Ox-LDL signal is important in determining the time scales of the problem. $\lambda_0(0)$ is always positive in (4.10). In the second term on the right-hand side of (4.11), the exponential and sine functions are always positive: it is clear that the integral will be negative if X_0 is sufficiently close to 1. Providing the boundary term $2L'(\tau_{\text{ext}})/\Delta\tau$ is sufficiently small, $\lambda_0(\mu)$ will be a decreasing function of μ if $\mu \ll 1$; in general, Fig. 10(a) suggests that this is also true for $\mu = O(1)$. Sufficiently large values of μ could cause the system to be unstable, resulting in exponentially growing solutions. For this to happen, μ must be taken large enough so that $\lambda_0 < 0$. In this case, cell death is not quick enough to compensate for the large numbers of new cells entering the plaque and in the absence of finite size effects, the macrophage density is predicted to rapidly increase, leading to a concomitant increase of debris through (3.36). High concentrations of debris weaken the overall integrity of the plaque and could quickly result in a rupture and heart attack. Finally, note that in Fig. 10(a), we take $\gamma_{\max} = 1$. With the approximation $\gamma \approx \gamma_{\max}$, the eigenvalues given by (4.9–4.11) are simply shifted when $\gamma_{\max}$ changes. In particular, $\lambda_0 \to \lambda_0 + \Delta\gamma_{\max}$ when $\gamma_{\max} \to \gamma_{\max} + \Delta\gamma_{\max}$. Hence, the eigenvalues for larger, more realistic $\gamma_{\max}$ can be easily inferred from Fig. 10(a).

Fig. 10(b) illustrates how λ_0 depends on the domain size, characterized by the intima width $\Delta P \equiv P_2 - P_1$ (with P_1 and P_2 defined in (3.28) and (3.29)) and hypoxic death rate $\gamma_{\max}$. For thicker arteries, the inflammation time scale T_c becomes larger. However, this effect rapidly saturates for very thick arteries ($\Delta P \gg 1$) with the saturation value being well approximated by $\gamma_{\max}$—see (4.9) and (4.10) with $\mu = 0$. The time to reach steady state is shorter when cells die rapidly of hypoxia. The functional dependence on domain size and death rate is well approximated by our 1D model through (4.9–4.11).

Finally, in Fig. 10(c), we see the dependence of λ_0 on the oxygen consumption rate r and on C_{crit}, which controls the resistance of macrophages to hypoxia (a smaller C_{crit} corresponds to stronger resistance to a low O_2 environment). We see that for realistic values of r, the inflammation time T_c is, again, well approximated by $1/\gamma_{\max}$. If cells are more resistant to hypoxia or if plaques are better oxygenated, then T_c increases and necrosis slows down.

So far, we have only discussed the time required for Q to reach its steady state. How does T_c affect the time for necrotic cores to form? In (3.35) and (3.36), Q evolves independently and R is coupled to Q via the γQ term. Let us study two limiting cases for the evolution. First, consider $0 < \lambda_0 \ll 1$. Then, Q finds its steady state very slowly. Because the density of dead cells R is slaved to a slowly varying Q and evolves on the same (slow) time scale, we also expect necrotic cores to form after a time $T_c = 1/\lambda_0$. When $\lambda = 0.01$ for example the physical time for core formation would be $(\tilde{\beta}_1 \lambda_0)^{-1} \approx 3$ years. Bearing in mind that $\gamma_{\max} \approx 120$ in most situations (see Table 2), can λ_0 really attain such small values? From Fig. 10(a), we see that λ_0 can be small and positive providing $\mu \gg \gamma_{\max}$ and Ox-LDL is present sufficiently deep within the intima ($\chi \sim 1$). However, μ must not be so large that $\lambda_0 < 0$, otherwise plaque rupture quickly ensues. In our linear model, slow necrosis appears to be a very special case. Now,

consider $\lambda_0 \gg 1$ which is the case whenever $\gamma_{\max}$ is large and chemotaxis is relatively unimportant. From (4.10), the time scale for macrophages to find their steady state is then $T_c \approx 1/\gamma_{\max} \ll 1$. In (3.36), the time scale of evolution for the dead cell density is now $O(1)$ and cores form after about $1/\tilde{\beta}_1 \approx 10$ days: a gross underestimate given that vulnerable plaques typically take decades to develop.

There are several reasons for the discrepancy between our simulations and real plaques. First, it is possible that conditions inside a plaque are not as hypoxic as presumed. Many plaques in their later stages develop vasa vasorum: smaller blood vessels that provide oxygen for the cells of larger blood vessels. An intima that contains a dense network of vasa vasorum could therefore have a smaller effective $\gamma_{\max}$ and therefore larger T_c. The necrotic core would also develop on this new, slower time scale. Second, our value for $\tilde{\beta}_1$ in Table 1 was estimated to be 0.1 per day. If the dead cell removal rate was much slower than our estimated value, the time scale of the plaque growth would become much larger. Third, in our model, we assumed a time-independent Ox-LDL concentration L. In reality, diet and exercise could affect the levels of Ox-LDL within the plaque. When a plaque has low levels of Ox-LDL, the transformation from macrophage to foam cell should be suppressed. Since foam cells are less able to access the oxygen supply than macrophages, they are primarily responsible for nucleating the necrotic core. Therefore, necrotic matter within the core should dissipate at a rate $\tilde{\beta}_1$ when there is no Ox-LDL present. If there are many Ox-LDL free periods distributed throughout the lifetime of the plaque, necrosis could take much longer to develop than our model predicts. Finally, although vulnerable plaques are usually found in people aged 50 and over, the transition from a fatty streak or intimal thickening to a TCFA does not necessarily have to take decades. Recall that our original aim was to explore the change from an innocuous plaque to a vulnerable one. It is certainly possible for fatty streaks or intimal thickenings to remain dormant for long periods of time with the transition to TCFA occurring over several years as opposed to decades—this time span could probably be predicted by our model with minor modifications to account for (say) the presence of vasa vasorum and time-dependent Ox-LDL.

5. Conclusions

In this paper, we explored a linear model for necrotic core growth in a vulnerable plaque with a focus on changes in composition. Our model included the effects of macrophage diffusion, death and chemotaxis: monocytes adhere to the endothelium (Fig. 2(c)) and enter the intima where they become macrophages. The macrophages move by a combination of random motion and chemotaxis towards the source of Ox-LDL, die due to lack of oxygen and nucleate the necrotic core (Fig. 2(d)). We studied our equations in 2D arterial cross sections and neglected changes in the plaque in the direction along the blood vessel. We did not account for the effects of remodelling or mechanical stress.

Our model predicts the development of crescent-shaped necrotic cores, which are commonly observed in ultrasound images and stained cross sections (see Fig. 2(d)). It also confirms some clinical observations, e.g. (i) regions of inflammation are closely correlated with regions of necrosis, (ii) plaques are heavily infiltrated with macrophages before necrotic cores form and (iii) over the course of plaque growth, macrophages are mainly confined near the lumen, within a plaque 'cap'. We also found that since the macrophage death rate is high far from the lumen, it is difficult for regions deep in the intima to become inflamed for any significant amount of time. Hence, in the absence of vasa vasorum and other oxygen sources, arteries with large cross-sectional areas (i.e. those that have undergone extensive outward remodelling) should have relatively small necrotic fractions, whereas in blood vessels with smaller areas, the necrotic core could — according to our calculations — easily occupy most of the artery.

Because our model is linear and autonomous, its evolution to steady state can be found exactly in terms of its eigenfunctions and eigenvalues. The time scale for core development is estimated by

examining the smallest eigenvalue. We calculated the eigenvalues for macrophage evolution and determined their dependence on system parameters such as chemotactic coefficient, death rate and oxygen levels. We found that for the estimated plaque parameters and a constant-in-time Ox-LDL distribution, the evolution to steady state occurs very rapidly, on the order of a few weeks. This is a weakness of our model because plaques are thought to develop over the course of many years or even decades. One possible way to improve our model in this respect is to explicitly include the effect of vessel expansion (remodelling). A healthy artery is usually concentric with a thin intimal region. As the vessel becomes more diseased, the intima becomes thicker as cells accumulate. Necrotic cores form once the thickness exceeds the diffusion length of oxygen. Since remodelling occurs very slowly (possibly over decades), cores would also only nucleate on this same time scale.

In the context of existing modelling efforts of plaques, we see our work as being complementary to studies of mechanical stress distributions (e.g. see Vengrenyuk *et al*., 2006; Baldewsing *et al*., 2004). In these papers, inhomogeneities in the plaque (e.g. lipid pools, micro-calcifications) yield stress profiles that are computed using the finite element method or analytic methods. Usually the inhomogeneities are static. In contrast, the main concern in our model is with how cores develop over time and how long these time scales are. How would the inclusion of mechanics into our model affect the predictions? There is evidence to suggest that the flux of LDL into the intima is increased when arterial wall stress is increased (Thubrikar, 2007). This could, in turn, increase the concentration of Ox-LDL in the intima and speed up cell death and necrosis. Excessive stresses within the artery could also cause tissue damage, which would illicit a proliferative response from SMCs. The eventual result would probably be a greater number of cells within the intima, more cell death and therefore larger necrotic cores.

Another extension is to add more detailed biochemistry. In Fig. 1, we see many processes that influence plaque growth. Two important factors that we have neglected in our model are the production of mineral deposits by SMCs and the creation of lipid pools from the macrophages' metabolism. In principle, it should not be difficult to supplement our existing PDEs with equations for the infiltration of SMCs and their creation of calcification, and to include the effects of lipid production by macrophages.

REFERENCES

Acierno, L. J. (1994) *The History of Cardiology*. New York: Parthenon Publishing Group.

Alberts, B., Johnson, A., Lewis, J., Raff, M., Roberts, K. & Walter, P. (2008) *Molecular Biology of the Cell*, 5th edn. New York: Garland Science.

Anitschkow, N. & Chalatow, S. (1913) On experimental cholesterin steatosis and its significance in the origin of some pathologic processes. *J. Gen. Pathol. Pathol. Anat.*, **24**, 1–9.

Bailey, A. M., Thorne, B. C. & Peirce, S. M. (2007) Multi-cell agent-based simulation of the microvasculature to study the dynamics of circulating inflammatory cell trafficking. *Ann. Biomed. Eng.*, **35**, 916–936.

Baldewsing, R. A., de Korte, C. L., Schaar, J. A., Mastik, F. & van der Steen, A. F. W. (2004) Finite element modelling and intravascular ultrasound elastography of vulnerable plaques: parameter variation. *Ultrasonics*, **42**, 723–729.

Byrne, H. M. (2010) Dissecting cancer through mathematics: from the cell to the animal model. *Nat. Rev. Cancer*, **10**, 221–230.

Calvez, V., Houot, J. G., Meunier, N., Raoult, A. & Rusnakova, G. (2010) Mathematical and numerical modelling of early atherosclerotic lesions. *ESAIM Proc.*, **30**, 1–15.

Chatzizisis, Y. S., Coskun, A. U., Jonas, M., Edelman, E. R., Feldman, C. L. & Stone, P. H. (2007) Role of endothelial shear stress in the natural history of coronary atherosclerosis and vascular remodelling: molecular, cellular, and vascular behaviour. *J. Am. Coll. Cardiol.*, **49**, 2379–2393.

Davies, M. J. (1992) Anatomic features in victims of sudden coronary death: coronary artery pathology. *Arterioscler. Thromb. Vasc. Biol.*, **85**, 119–124.

Greenspan, H. P. (1972) Models for the growth of a solid tumour by diffusion. *Stud. Appl. Math.*, **4**, 317–340.

Henrikson, T., Mahoney, E. M. & Steinberg, D. (1981) Enhanced macrophage degradation of low density lipoprotein previously incubated with cultured endothelial cells: recognition by receptors for acetylated low density lipoproteins. *Proc. Nat. Acad. Sci. U.S.A.*, **78**, 6499–6503.

Hlatky, L., Sachs, R. K. & Alpen, E. L. (1988) Joint oxygen-glucose deprivation as the cause of necrosis in a tumour analog. *J. Cell. Physiol.*, **134**, 167–178.

Hsiai, T. K., Cho, S. K., Reddy, S., Hama, S., Navab, M., Demer, L. L., Honda, H. M. & Ho, C. H. (2001) Pulsatile flow regulates monocyte adhesion to oxidized lipid-induced endothelial cells. *Arterioscler. Thromb. Vasc. Biol.*, **21**, 1770–1776.

Ibragimov, A. I., McNeal, C. J., Ritter, L. R., & Walton, J. R. (2005) A mathematical model of atherogenesis as an inflammatory response. *Math. Med. Biol.*, **22**, 305–33.

Keener, J. & Sneyd, J. (2009a) *Mathematical Physiology I: Cellular Physiology*. New York: Springer.

Keener, J. & Sneyd, J. (2009b) *Mathematical Physiology II: Systems Physiology*. New York: Springer.

Keller, E. F. & Segel, L. A. (1971) Models for chemotaxis. *J. Theor. Biol.*, **30**, 225–234.

Korn, C. B. & Schwarz, U. S. (2008) Dynamic states of cells adhering in shear flow: From slipping to rolling. *Phys. Rev. E*, **77**, 041904.

Ma, Y., Wang, J., Liang, S., Dong, C. & Du, Q. (2010) Application of population dynamics to study heterotypic cell aggregations in the near-wall region of a shear flow. *Cell. Mol. Bioeng.*, **3**, 3–19.

Majno, G. & Joris, I. (1995) Apoptosis, oncosis and necrosis. *Am. J. Pathol.*, **146**, 3–15.

Mehta, S. K., McCrary, J. R., Frutkin, A. D., Dolla, W. J. S. & Marso, S. P. (2007) Intravascular ultrasound radiofrequency analysis of coronary atherosclerosis: an emerging technology for the assessment of vulnerable plaque. *Eur. Heart J.*, **28**, 1283–1288.

Nishi, K., Itabe, H., Uno, M., Kitazato, K. T., Horiguchi, H., Shinno, K. & Nagahiro, S. (2002) Oxidized LDL in carotid plaques and plasma associates with plaque instability. *Arterioscler. Thromb. Vasc. Biol.*, **22**, 1649 – 1654.

Ougrinovskaia, A., Thompson, R. S. & Myerscough, M. R. (2010) An ODE model of early stages of atherosclerosis: mechanisms of the inflammatory response. *Bull. Math. Biol.*, **72**, 1534–1561.

Owen, M. R., Byrne, H. M. & Lewis, C. E. (2004) Mathematical modelling of the use of macrophages as vehicles for drug delivery to hypoxic tumour sites. *J. Theor. Biol.*, **226**, 377–391.

Painter, K. J. & Hillen, T. (2002) Volume-filling and quorum-sensing in models for chemosensitive movement. *Can. Appl. Math. Q.*, 501–543.

Ross, R. (1986) The pathogenesis of atherosclerosis. *N. Engl. J. Med.*, 488.

Shah, P. K. (2003) Mechanisms of plaque vulnerability and rupture. *J. Am. Coll. Cardiol.*, **41**, 15S–22S.

Shiffman, D., Mikita, T., Tai, J. T. N., Wade, D. P., Porter, J. G., Seilhamer, J. J., Somogyi, R., Liang, S. & Lawn, R. M. (2000) Large scale gene expression analysis of cholesterol-loaded macrophages. *J. Biol. Chem.*, **275**, 37324–37332.

Tegoulia, V. A. & Cooper, S. L. (2000) Leukocyte adhesion on model surfaces under flow: effects of surface chemistry, protein adsorption, and shear rate. *J. Biomed. Mater. Res.*, **50**, 291–301.

Thubrikar, M. J. (2007) *Vascular Mechanics and Pathology*. New York: Springer.

Tsimikas, S. & Witzum, J. L. (2000) The oxidative modification hypothesis of atherogenesis. *Oxidative Stress and Vascular Disease* (J. F. Keaney ed.). Norwell, MA: Kluwer Academic Publishers, pp. 49–74.

Van Hoydonck, P. G. A., Schouten, E. G. & Temme, E. H. M. (2003) Reproducibility of blood markers of oxidative status and endothelial function in healthy individuals. *Clin. Chem.*, **49**, 963–965.

Vengrenyuk, Y., Carlier, S., Xanthos, S., Cardoso, L., Ganatos, P., Virmani, R., Einav, S., Gilchrist, L. & Weinbaum S. (2006) A hypothesis for vulnerable plaque rupture due to stress-induced debonding around cellular microcalcifications in thin fibrous caps. *Proc. Nat. Acad. Sci. U.S.A.*, **103**, 14678–14683.

Virmani, R., Kolodgie, F. D., Burke, A. P., Farb, A. & Schwartz, S. M. (2000) Lessons from sudden coronary death: a comprehensive morphological classification scheme for atherosclerotic lesions. *Arterioscler. Thromb. Vasc. Biol.*, **20**, 1262–1275.

Virmani, R., Narula, J., Leon, M. B. & Willerson, J. T. (eds) (2007) *The Vulnerable Atherosclerotic Plaque: Strategies for Diagnosis and Management*. Malden, MA: Blackwell.

Walpola, P. L., Gotlieb, A. I., Cybulsky, M. I. & Langille B. L. (1995) Expression of ICAM-1 and VCAM-1 and monocyte adherence in arteries exposed to altered shear stress. *Arterioscler. Thromb. Vasc. Biol.*, **15**, 2–10.

Zohdi, T. I., Holzapfel, G. A. & Berger, S. A. (2004) A phenomenological model for atherosclerotic plaque growth and rupture. *J. Theor. Biol.*, **227**, 437–443.

Appendix A. Parameter values

Here we explain how the parameter values in Table 1 were calculated. In many cases, values that are specific to plaques could not be found and were estimated from other systems (e.g. the oxygen consumption rate for macrophages is taken as the one for tumour cells in necrosis experiments). The resulting dimensionless constants in Table 2 were used as guidelines for the simulations.

1. Macrophage attachment rate, $\tilde{k}$: This value is for neutrophil attachment onto carboxyl-terminated gold monolayers. Figure 4 of Tegoulia & Cooper (2000) reports a cell flux of 150 cells/mm^2 in 10 min for a shear rate of 100/s. Since the neutrophil concentration was 10^5 cells/mL, the attachment rate $\tilde{k}$ is calculated as 2.5×10^{-4} cm/s or about 20 cm/day.

2. Macrophage Diffusivity within a plaque, $\tilde{\nu}_1$: This value, taken from Keener & Sneyd (2009b) chapter 13.4.2., represents the typical diffusivity of leucocytes in tissue during an infection.

3. Oxygen diffusivity within a plaque, $\tilde{\nu}_3$: This value, taken from Keener & Sneyd (2009a) chapter 2.3.1, is the diffusion constant for molecular O_2 in muscle.

4. Dead cell removal rate $\tilde{\beta}_1$: If we assume that dead cells in the plaque are turned over about once every 10 days, we have a removal rate of about 0.1 cells/day.

5. Background oxygen consumption rate $\tilde{\beta}_2$: Oxygen consumption in muscle tissue that is at rest occurs at about 5×10^{-8} mol/cm^3/s and a typical concentration of O_2 in muscle is about 3.5×10^{-8} mol/cm^3. Both of these values are taken from Keener & Sneyd (2009a) chapter 2.3.1. Therefore, we calculate the consumption rate to be 1.4/s. This value is probably an upper bound for $\tilde{\beta}_2$.

6. Oxygen consumption rate of macrophages, $\tilde{\beta}_3$: In necrosis experiments on cancer cells (Hlatky *et al.*, 1988), the authors use equation (3.3) with $\tilde{\beta}_2 = 0$ and write the mass-action oxygen consumption term as $-\frac{N}{Z} Q_0$, where N is the number of tumour cells per unit area and Z is width of a channel occupied by the cells. Hence, N/Z is the cancer cell density corresponding to $\tilde{Q}$ in (3.3). Q_0 is the per-cell consumption rate of O_2, which they take as a Hill form: see (5) in the appendix of Hlatky *et al.* (1988). However when consumption is oxygen limited, we can take $Q_0 \sim bO/(\kappa B)$ where O is the oxygen concentration, $b \approx 1.5 \times 10^{-13}$ moles/cell-hour, $B = 0.19$ mM and $\kappa = 0.05$. Therefore, we identify $\tilde{\beta}_3$ with the quantity $b/(\kappa B) \approx 3.8 \times 10^{-4}$ cm^3/cell/day. This value is probably a lower bound for $\tilde{\beta}_3$.

7. 'Natural' macrophage death rate $\tilde{\gamma}_{\min}$: If we assume that the normal lifespan of macrophages is about 30 days, the macrophage death rate is 0.03 cells/day.

8. Hypoxic macrophage death rate $\tilde{\gamma}_{\max}$: If we assume that macrophages can survive for about 2 h in ischemic conditions before undergoing (non-apoptotic) cell death, the corresponding death rate is 12 cells/day.

9. Typical Ox-LDL concentration in plaque, $\tilde{L}_0$: Nishi *et al.* (2002) found that Ox-LDL concentrations inside a plaque were typically 10–14 ng of Ox-LDL per microgram of apolipoprotein B, about 70× greater than in blood plasma. Van Hoydonck *et al.* (2003) find the Ox-LDL concentration in blood to be 10 mg/L. Therefore, we take $\tilde{L}_0 = 0.7$ mg/cm^3.

10. Oxygen concentration in blood, $\tilde{C}_0$: The solubility of molecular O$_2$ in blood plasma is 1.4×10^{-6} M/mm Hg (Keener & Sneyd, 2009b, table 13.2, chapter 13.1). Assuming an arterial partial pressure of 40 mm Hg, the concentration of dissolved oxygen is 5.6×10^{-5} mol/L.

11. Monocyte concentration in blood, $\tilde{Q}_0$: This value is taken from Alberts *et al.* (2008, table 23-1, Chapter 23).

12. Hypoxic oxygen concentration, $\tilde{C}_{\mathrm{crit}}$: In Figure 2 of Owen *et al.* (2004), simulations of tumour growth were compared to *in vitro* tumours and a similar Hill form for the death rate in (3.4) was used. The authors found that when $C_{\mathrm{crit}} = 0.2$, the simulated growth of necrotic regions matched experiments.

Appendix B. Numerical methods

With bipolar coordinates

$$x = \frac{d \sinh \tau}{(\cosh \tau - \cos \sigma)}, \quad y = \frac{d \sin \sigma}{(\cosh \tau - \cos \sigma)}, \tag{B.1}$$

our domain of solution is $-\pi \leqslant \sigma < \pi$ and $\tau_{\mathrm{ext}} \leqslant \tau \leqslant \tau_{\mathrm{int}}$, corresponding to the region between eccentric circles with interior and exterior radii $a = 1$ and $b = d/\sinh \tau_{\mathrm{ext}}$, respectively. We solve the governing equations on a logically rectangular grid: (τ_i, σ_j), $i = 1, 2, \ldots M$, $j = 1, 2, \ldots N$ are defined by

$$\tau_i = \tau_{\mathrm{ext}} + (i - 1)\Delta\tau, \tag{B.2}$$

$$\sigma_j = -\pi + (j - 1)\Delta\sigma, \tag{B.3}$$

$$\Delta\tau = (\tau_{\mathrm{int}} - \tau_{\mathrm{ext}})/(M - 1), \tag{B.4}$$

$$\Delta\sigma = 2\pi/N. \tag{B.5}$$

Since solutions are periodic in σ, values at $\sigma = \pi$ are not directly calculated. We write the numerical approximation to $Q(\tau_i, \sigma_j)$, $R(\tau_i, \sigma_j)$ as $Q_{i,j}$, $R_{i,j}$, and for brevity of notation, arithmetic for the index j is done modulo N, e.g., $Q_{i,N+1} = Q_{i,1}$, $(\nabla R)_{i,0} = (\nabla R)_{i,N}$. The scale factor in our bipolar coordinate system is

$$h_{i,j} = d/(\cosh \tau_i - \cos \sigma_j). \tag{B.6}$$

B.1 *Evolution in time*

For $i = 2, \ldots, M - 1$, $j = 1, 2, \ldots, N$, (3.35) and (3.36) are discretized in space as

$$\dot{Q}_{i,j} = -\mu (\nabla Q \cdot \nabla L)_{i,j} - Q_{i,j} (\nabla^2 L)_{i,j} + \nu_1 (\nabla^2 Q)_{i,j} - \gamma_{i,j} Q_{i,j}, \tag{B.7}$$

$$\dot{R}_{i,j} = -\nu_2 (\nabla^2 R)_{i,j} + \gamma_{i,j} Q_{i,j} - R_{i,j}, \tag{B.8}$$

where $\gamma_{i,j} = \gamma (C_{i,j})$ and $C_{i,j}$ is calculated from (3.37). For a grid function $H_{i,j}$, its Laplacian and gradient are approximated by

$$(\nabla^2 H)_{i,j} = \frac{1}{h_{i,j}^2} \left(\frac{H_{i,j+1} - 2H_{i,j} + H_{i,j-1}}{(\Delta \sigma)^2} + \frac{H_{i+1,j} - 2H_{i,j} + H_{i-1,j}}{(\Delta \tau)^2} \right), \tag{B.9}$$

$$(\nabla H)_{i,j} = \frac{1}{h_{i,j}} \left[\frac{H_{i+1,j} - H_{i-1,j}}{2\Delta \tau}, \frac{H_{i,j+1} - H_{i,j-1}}{2\Delta \sigma} \right], \tag{B.10}$$

for $i = 2, \ldots, M - 1$, $j = 1, \ldots, N$. The PDEs for Q at the inner and outer boundaries $\tau = \tau_{\text{int}}, \tau_{\text{ext}}$ are discretized as

$$\dot{Q}_{1,j} = -\frac{1}{h_{1,j}} \left[\frac{-3F_{1,j}^{(\tau)} + 4F_{2,j}^{(\tau)} - F_{3,j}^{(\tau)}}{2\Delta \tau} + \frac{F_{1,j+1}^{(\sigma)} - F_{1,j-1}^{(\sigma)}}{2\Delta \sigma} \right] - \gamma_{1,j} Q_{1,j}, \tag{B.11}$$

$$\dot{Q}_{M,j} = -\frac{1}{h_{M,j}} \left[\frac{3F_{M,j}^{(\tau)} - 4F_{M-1,j}^{(\tau)} + F_{M-2,j}^{(\tau)}}{2\Delta \tau} + \frac{F_{M,j+1}^{(\sigma)} - F_{M,j-1}^{(\sigma)}}{2\Delta \sigma} \right] - \gamma_{M,j} Q_{M,j}, \tag{B.12}$$

for $j = 1, \ldots, N$, where the flux in the τ direction, $F^{(\tau)}$, is calculated using

$$F_{i,j}^{(\tau)} = \begin{cases} 0, & \text{if } i = 1, \\ -\nu_1 \left(\dfrac{Q_{i+1,j} - Q_{i-1,j}}{2h_{i,j}\Delta \tau} \right) + \mu Q_{i,j} \left(\dfrac{L_{i+1,j} - L_{i-1,j}}{2h_{i,j}\Delta \tau} \right), & \text{if } i = 2, 3, M - 2 \text{ or } M - 1, \\ k(Q_{i,j} - 1), & \text{if } i = M, \end{cases} \tag{B.13}$$

for $j = 1, \ldots N$. The flux in the σ direction, $F^{(\sigma)}$, is calculated using

$$F_{i,j}^{(\sigma)} = -\nu_1 \left(\frac{Q_{i,j+1} - Q_{i,j-1}}{2h_{i,j}\Delta \sigma} \right) + \mu Q_{i,j} \left(\frac{L_{i,j+1} - L_{i,j-1}}{2h_{i,j}\Delta \sigma} \right), \tag{B.14}$$

for $i = 1, M$ and $j = 1, \ldots N$. The PDEs that govern R at the boundaries are discretized in a similar way. Equations (B.7), (B.11), (B.12) and the corresponding equations for R form a system of coupled ordinary differential equations. They were solved numerically using Matlab's ode15s routine on a $M \times N = 30 \times 30$ grid with absolute tolerance 10^{-4} and relative tolerance 10^{-2}. We then used spline interpolation to a (300×300) grid to plot the results.

B.2 *Eigenvalue problem*

The time evolution of the solution into its steady-state form is governed by the solution to the homogeneous system

$$\dot{Q}(\tau, \sigma, t) + S[Q(\tau, \sigma, t)] = 0, \tag{B.15}$$

with boundary conditions

$$-\nu_1 \frac{\partial Q}{\partial \tau} + \mu Q \frac{\partial L}{\partial \tau} = kQ, \quad \text{on } \tau = \tau_{\text{int}}, \tag{B.16}$$

$$-\nu_1 \frac{\partial Q}{\partial \tau} + \mu Q \frac{\partial L}{\partial \tau} = 0, \quad \text{on } \tau = \tau_{\text{ext}}, \tag{B.17}$$

and 2π periodicity in σ. The operator S is

$$S[u] = -\nu_1 \nabla^2 u + \mu \nabla \cdot (u \nabla L) + \gamma(\tau, \sigma) u. \tag{B.18}$$

The solution to (B.15–B.18) is $Q(\tau, \sigma, t) = \sum_{n=0}^{\infty} A_n \exp(-\lambda_n t) Q_n(\tau, \sigma)$ for some constants A_n, where the eigenfunctions Q_m and eigenvalues λ_m satisfy

$$S[Q_m] = \lambda_m Q_m. \tag{B.19}$$

To solve for Q_m and λ_m numerically, S and the boundary conditions were discretized in a similar fashion to Section (B.1) and Matlab's eigs routine was used to find the first few eigenvalues and eigenfunctions. A typical mesh size was $(M, N) = (30, 300)$. Eigenfunctions were interpolated onto a 500×300 mesh in Fig. 9.

Appendix C. Necessary condition for unbounded solutions

Given that $\mu \geqslant 0$, we show that the origin of unbounded solutions stems from chemotaxis. If we multiply (3.35) by Q, integrate over the whole domain and use boundary conditions (3.39) and (3.40), we obtain

$$\frac{\mathrm{d}}{\mathrm{d}t} \iint \frac{Q^2}{2} \, \mathrm{d}A = -k \oint_{\tau = \tau_{\text{int}}} Q(Q - 1) \mathrm{d}s - \iint \left[\nu_1 |\nabla Q|^2 - \mu Q \nabla L \cdot \nabla Q + \gamma(\tau, \sigma) Q^2 \right] \mathrm{d}A.$$

On the right-hand side, the first term represents the kinetic contribution from macrophage attachment at the inner boundary. This term is negative for sufficiently large Q and is therefore stabilizing. The first term in the integral that stems from diffusion is stabilizing. The third term is also stabilizing since the death rate γ is always positive. The second term is the only one that can destabilize the system. Hence, if solutions become unbounded, we must have $\mu > 0$.

Appendix D. Perturbed eigenvalues for 1D model

We approximate (4.1) with the simpler 1D problem

$$-\nu_1 \frac{\mathrm{d}^2 Q}{\mathrm{d}\tau^2} + (\gamma_{\text{max}} - \lambda) Q = -\mu \frac{\mathrm{d}(Qg(\tau))}{\mathrm{d}\tau}, \tag{D.1}$$

$$g(\tau) = -\frac{2(\tau - \tau_0)}{\delta^2} \exp\left[-(\tau - \tau_0)^2/\delta^2\right], \tag{D.2}$$

where $\tau_{\mathrm{int}} < \tau < \tau_{\mathrm{ext}}$, $g(\tau) \equiv L'(\tau)$ and we have dropped the spatial dependence in the death rate. We also take $k \to \infty$ so that the boundary conditions simplify to

$$Q = 0, \quad \text{on } \tau = \tau_{\mathrm{int}}, \tag{D.3}$$

$$-\nu_1 \frac{\mathrm{d}Q}{\mathrm{d}\tau} + \mu Q g = 0, \quad \text{on } \tau = \tau_{\mathrm{ext}}. \tag{D.4}$$

Assuming $\mu \ll 1$, we carry out an asymptotic analysis to understand the effect of a small amount of chemotaxis on the eigenvalues, and hence on the time scales of the problem. We expand Q and λ using regular perturbation series

$$Q = Q^{(0)} + \mu Q^{(1)} + O(\mu^2), \tag{D.5}$$

$$\lambda = \lambda^{(0)} + \mu \lambda^{(1)} + O(\mu^2). \tag{D.6}$$

At $O(1)$, Q_0 and λ_0 satisfy

$$-\nu_1 \mathrm{d}^2 Q^{(0)}/\mathrm{d}\tau^2 + (\gamma_{\max} - \lambda^{(0)}) Q^{(0)} = 0, \tag{D.7}$$

$$Q^{(0)}(\tau_{\mathrm{int}}) = 0, \tag{D.8}$$

$$\mathrm{d}Q^{(0)}(\tau_{\mathrm{ext}})/\mathrm{d}\tau = 0, \tag{D.9}$$

so that

$$Q^{(0)}(\tau) = Q_n^{(0)}(\tau) = \sin\left(\frac{(n+1/2)\pi}{\Delta\tau}(\tau - \tau_{\mathrm{int}})\right), \tag{D.10}$$

$$\lambda^{(0)} = \lambda_n^{(0)} = \gamma_{\max} + \nu_1 \left(\frac{(n+1/2)\pi}{\Delta\tau}\right)^2, \tag{D.11}$$

for $n = 0, 1, 2, \ldots$, where $\Delta\tau = \tau_{\mathrm{ext}} - \tau_{\mathrm{int}}$. At $O(\mu)$, $Q^{(1)}$ satisfies

$$-\nu_1 \mathrm{d}^2 Q^{(1)}/\mathrm{d}\tau^2 + \left(\gamma_{\max} - \lambda_n^{(0)}\right) Q^{(1)} = \lambda^{(1)} Q_n^{(0)} - (Q_n^{(0)} g)'. \tag{D.12}$$

Expanding $Q^{(1)}$ in terms of the eigenfunctions of the $O(1)$ problem, we take $Q^{(1)}(\tau) = \sum_{m=0}^{\infty} c_m Q_m^{(0)}(\tau)$ so that

$$\sum_{m=1}^{\infty} c_m \left(\lambda_m^{(0)} - \lambda_n^{(0)}\right) Q_m^{(0)}(\tau) = \lambda^{(1)} Q_n^{(0)} - (Q_n^{(0)} g)'. \tag{D.13}$$

Multiplying both sides by $Q_n^{(0)}(\tau)$ and integrating from τ_{int} to τ_{ext}, we obtain

$$\lambda^{(1)} = \lambda_n^{(1)} = \frac{2}{\Delta\tau} \int_{\tau_{\mathrm{int}}}^{\tau_{\mathrm{ext}}} Q_n^{(0)} \left(Q_n^{(0)} g\right)' \mathrm{d}\tau. \tag{D.14}$$

Our final expression for the nth perturbed eigenvalue when $\mu \ll 1$ is

$$\lambda_n = \lambda_n^{(0)} + \mu \lambda_n^{(1)} + O(\mu^2), \tag{D.15}$$

where

$$\lambda_n^{(0)} = \gamma_{\max} + \nu_1 \left(\frac{(n + 1/2)\pi}{\Delta \tau} \right)^2, \tag{D.16}$$

$$\lambda_n^{(1)} = \frac{2}{\Delta \tau} L'(\tau_{\text{ext}}) \tag{D.17}$$
$$+ \frac{(2n + 1)\pi}{\delta^2} \int_0^1 (X - X_0) \exp\left[-\frac{\Delta \tau^2}{\delta^2} (X - X_0)^2 \right] \sin\left[(2n + 1)\pi X \right] dX,$$

and $X_0 = (\tau_0 - \tau_{\text{int}})/\Delta \tau$.